

SCIPP 99/39
September 1999

PRECISE ELECTROWEAK MEASUREMENTS AT THE Z^0 POLE

BRUCE A. SCHUMM
Institute for Particle Physics
University of California, Santa Cruz

Over the last decade, precise LEP and SLC measurements of electroweak coupling parameters at the Z^0 pole have lead to tests of the Standard Model to unprecedented precision. This report presents a comprehensive review of these studies, including a review of relevant Z^0 pole physics issues, facilities, instrumentation, and the measurements made. Global fits for the Higgs Boson mass and $Z^0 - b$ coupling parameters are also presented.

Talk presented at the 1999 Conference on Physics In Collision, Anne Arbor,
Michigan, June 24–26, 1999

PRECISE ELECTROWEAK MEASUREMENTS AT THE Z^0 POLE

B. A. SCHUMM

University of California, Santa Cruz, CA 95064, USA

E-mail: schumm@scipp.ucsc.edu

Over the last decade, precise LEP and SLC measurements of electroweak coupling parameters at the Z^0 pole have lead to tests of the Standard Model to unprecedented precision. This report presents a comprehensive review of these studies, including a review of relevant Z^0 pole physics issues, facilities, instrumentation, and the measurements made. Global fits for the Higgs Boson mass and $Z^0 - b$ coupling parameters are also presented.

1 Introduction

With the end of the SLC/SLD run at SLAC in June, 1998, the era of precision tests of the standard model using e^+e^- beams tuned to the energy of the Z^0 -boson resonance came to a close, at least for the foreseeable future. Within the decade since the first production in 1988 of the Z^0 with lepton beams, however, the precision of the resulting constraints on the phenomenology of the Standard Model has exceeded even the more optimistic estimates put forth at the beginning of the running. While no clear disagreements with the Standard Model have come to light during this period, the development of the Standard Model and its subsequent confirmation at the 1-loop level, to accuracies exceeding one part in 10^{-3} , surely stands as one of the great achievements of human scientific pursuit.

2 Standard Model Background

Precise tests of the Standard Model at the Z^0 pole are performed via measurements of the couplings of the various fermions to the Z^0 , and primarily through the quantitative extent of parity violation in those couplings. In the Standard Model, the neutral components of the parity-violating $SU(2)_L$ and partially parity-conserving $U(1)$ interactions are mixed according to an angle θ_W , the ‘weak mixing angle’. The resulting physical states are the weak Z^0 boson and the electromagnetic γ , the latter of which mediates a purely parity conserving interaction, while the Z^0 thus mediates a partially parity-violating interaction. The quantitative extent of the Z^0 parity violation thus depends on the value of θ_W , as well as the electric (Q) and weak isospin (t_3) charges

Table 1. Standard Model Couplings and Parity Violation (assuming $\sin^2 \theta_W = 0.231$)

Fermion	t_3^f	Q^f	g_L^f	g_R^f	A_f	$dA_f/d\sin^2 \theta_W$
e, μ, τ	-1/2	-1	-0.269	0.231	0.151	-7.8
ν	+1/2	0	0.500	0.000	1.000	-0.0
d, s, b	-1/2	-1/3	-0.423	0.077	0.935	-0.6
u, c, t	+1/2	+2/3	0.346	-0.154	0.669	-3.5

$$m_J = -1$$

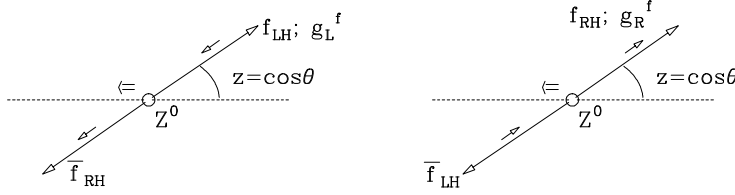


Figure 1. Decay of an $m_J = -1$ Z^0 boson into left- and right- handed fermions.

of the interacting fermion. Specifically, in terms of the left- and right-handed Z^0 -fermion couplings g_L^f and g_R^f , the quantitative extent of parity violation is expressed via the parity-violation parameters A_f :

$$A_f = \frac{(g_L^f)^2 - (g_R^f)^2}{(g_L^f)^2 + (g_R^f)^2} \quad (1)$$

where $g_L^f = t_3^f - Q^f \sin^2 \theta_W$ and $g_R^f = -Q^f \sin^2 \theta_W$. Table 1 shows the electroweak charges, couplings and parity violation parameters A_f for the various fermion species. Also shown is the resulting sensitivity to the weak mixing angle. It is seen that the extent of parity violation in the coupling of the Z^0 to charged leptons is very sensitive to the value of $\sin^2 \theta_W$, and thus to the vacuum polarization effects which renormalize the boson propagator. On the other hand, the extent of parity violation to down-type quarks is quite insensitive to $\sin^2 \theta_W$, and thus measurements of parity violation in these couplings are interesting in that they constrain $Z^0 - f$ vertex corrections independently of the propagator effects which renormalize $\sin^2 \theta_W$.

The angular differential cross-section for fermion production at the Z^0

pole is given by

$$\frac{d\sigma^f}{dz} \propto (1 - A_e P_e)(1 + z^2) + 2A_f(A_e - P_e)z, \quad (2)$$

where P_e is the longitudinal polarization of the electron beam, and $z = \cos \theta$. This relation can be understood entirely from angular momentum arguments. Figure 1 shows that the angular cross section for an $m_J = -1$ Z^0 boson decaying to a LH fermion and RH antifermion will be proportional to square of the spin-1 rotation matrix element corresponding to the transformation between an $m_J = -1$ state with spin projection on the z axis and an $m_J = -1$ state with spin projection along an axis rotated by $\cos \theta$ relative to the z axis: ¹

$$\sigma_{LH}^{m_J=-1} \propto |d_{-1,-1}^{(1)}(z)|^2 = (1 + z)^2. \quad (3)$$

For decay into a RH fermion, the argument is identical up to the substitution of $m_J = +1$ for the spin projection onto the rotated axis:

$$\sigma_{RH}^{m_J=-1} \propto |d_{+1,-1}^{(1)}(z)|^2 = (1 - z)^2. \quad (4)$$

Since the LH and RH coupling strengths are just g_L and g_R , we have for an $m_J = -1$ Z^0 sample:

$$\sigma_{tot}^{m_J=-1}(z) \propto g_L^2(1 + z)^2 + g_R^2(1 - z)^2 = (g_L^2 + g_R^2)(1 + z^2) + 2(g_L^2 - g_R^2)z. \quad (5)$$

The presence of the term odd in z leads to a forward-backward asymmetry in the overall fermion production rate, provided that $|g_L| \neq |g_R|$, i.e., that parity is violated. With a purely left-handed electron beam ($P_e = -1$), the sample of produced Z^0 bosons would be purely $m_J = -1$, and the forward-backward asymmetry would be

$$A_{FB}^{m_J=-1}(z) = \frac{\sigma^f(z) - \sigma^f(-z)}{\sigma^f(z) + \sigma^f(-z)} = \frac{g_L^2 - g_R^2}{g_L^2 + g_R^2} \frac{2z}{1 + z^2} = A_f \frac{2z}{1 + z^2} \quad (6)$$

where A_f is the parity violation parameter for fermion species f introduced above. However, by reproducing the above arguments for the case of $m_J = +1$, it's easy to see that the sign of the asymmetry flips. Thus, a forward-backward asymmetry develops only if there are *different numbers* of $m_J = +1$ and $m_J = -1$ Z^0 's in the overall sample. For an unpolarized electron beam (equal numbers of LH and RH electrons), this will only be true to the extent that the LH and RH couplings of the *electron* differ. Thus, the unpolarized forward-backward asymmetry also depends upon the extent A_e of parity violation in the Z^0 - e coupling:

$$A_{FB}^f(z) = \frac{\sigma^f(z) - \sigma^f(-z)}{\sigma^f(z) + \sigma^f(-z)} = A_e A_f \frac{2z}{1 + z^2}, \quad (7)$$

in agreement with Eqn. (2). By convention, this observable is usually expressed in terms of the integrated forward ($z > 0$) and backward ($z < 0$) cross sections:

$$A_{FB}^f = \frac{\sigma_F^f - \sigma_B^f}{\sigma_F^f + \sigma_B^f} = \frac{3}{4} A_e A_f. \quad (8)$$

where $\sigma_F^f = \int_0^1 \sigma^f(z) dz$ and $\sigma_B^f = \int_0^1 \sigma^f(-z) dz$.

2.1 Polarized Electron Beams

With a polarized electron beam, parity violation in the Z^0 - e coupling can be measured directly by forming the asymmetry A_{LR} in the left- and right-handed Z^0 production cross sections:

$$A_{LR} = \frac{\sigma_{e_L^- e^+} - \sigma_{e_R^- e^+}}{\sigma_{e_L^- e^+} + \sigma_{e_R^- e^+}} = \frac{(g_L^e)^2 - (g_R^e)^2}{(g_L^e)^2 + (g_R^e)^2} = A_e. \quad (9)$$

The sensitivity of this parameter to $\sin^2 \theta_W$ (see Table 1), combined with the indifference of the quantity to the particular final state fermion, render this the single most accurate approach to the measurement of $\sin^2 \theta_W$.

It is also possible to form a polarized *final-state* asymmetry

$$\tilde{A}_{FB}^f(z) = \frac{[\sigma_L^f(z) - \sigma_L^f(-z)] - [\sigma_R^f(z) - \sigma_R^f(-z)]}{\sigma_L^f(z) + \sigma_L^f(-z) + \sigma_R^f(z) + \sigma_R^f(-z)} = A_f \frac{2z}{1+z^2}. \quad (10)$$

Unlike its unpolarized counterpart, this observable is sensitive to *final state* parity violation alone. In the case $f = b$, this provides a direct constraint on Z^0 - b vertex effects, independent of the propagator effects which alter the value of $\sin^2 \theta_W$ (see Table 1).

Both of these observables, however, are mitigated by incomplete beam polarization ($|P_e| \neq 1$) according to

$$A_{meas} = |P_e| A_{true}.$$

Thus, in order to measure these observables accurately, it is necessary to have an electron beam with a large and well-measured polarization.

2.2 Z^0 Lineshape Parameters

At Born level, the total cross section for the production of fermion type f is given by

$$\sigma_{e^+ e^- \rightarrow f \bar{f}}(s) = \frac{12\pi}{M_Z^2} \frac{s \Gamma_{e^+ e^-} \Gamma_{f \bar{f}}}{(s - M_Z^2)^2 + s^2 \Gamma_Z^2 / M_Z^2} \quad (11)$$

where s is the square of the cms energy, and the partial width $\Gamma_{f\bar{f}}$ is given by

$$\Gamma_{f\bar{f}} = 2c_f[(g_L^f)^2 + (g_R^f)^2] \frac{G_F M_Z^3}{12\sqrt{2}\pi}. \quad (12)$$

Thus, measurements of the Z^0 resonance parameters M_Z , Γ_Z , and the peak cross section σ^0 , are important for constraining the Standard Model. In particular, the relation

$$\sin 2\theta_W = \left[\frac{4\pi\alpha_{\text{em}}}{\sqrt{2}G_F M_Z^2} \right]^{1/2} \quad (13)$$

exhibits the value of a precise measurement of M_Z , given our precise knowledge of α_{em} and G_F . With the value of θ_W thus constrained, measurements of $\sin^2 \theta_W$ via parity violation become exacting consistency checks of the Standard Model.

Finally, it should be pointed out that the discussion presented so far is strictly true only at Born level. At higher orders, radiative corrections act to change these relations somewhat. This is precisely what makes precision measurements interesting, in that new physics in radiative loops will potentially yield values for the observables in disagreement with Standard Model expectations. On the other hand, ‘uninteresting’ radiative corrections, to the extent that they are not empirically constrained, can enter in to obscure the above relations. As will be seen below, a particularly important example of this is the scale dependence of α_{em} , which receives contributions from intermediate-energy non-perturbative hadronic loops and thus is not known to arbitrary precision.

3 Z^0 Peak Facilities

Over the past decade, Z^0 peak running has been done at two facilities: the LEP electron-positron storage ring collider at CERN, and the SLC linear collider at SLAC. Table 2 shows the relative sample sizes (summed over the four LEP detectors) at the two facilities.

The SLC electron beam polarization, as discussed above, greatly increases the information content per hadronic event for many precision measurements, making the two facilities roughly comparable and nicely complementary. In addition, the small luminous region of the SLC (roughly $2 \mu\text{m} \times 0.7 \mu\text{m}$ for the SLC, *vs.* $250 \mu\text{m} \times 5 \mu\text{m}$ for LEP), as well as the smaller SLC interaction region beampipe radius (2.5 cm *vs.* 5.5 cm) give the SLC an intrinsic advantage for measurements making use of precision tracking – particularly those involving the production and decay of heavy flavor.

Table 2. Sample Sizes (No. of Hadronic Z^0 's) and Beam Polarization for the LEP and SLC Colliders

Year	LEP Sample $\times 10^{-3}$	SLC Sample $\times 10^{-3}$	$\langle P_e \rangle$ for the SLC
1988	0	0.5	0.0%
1989	0	0.3	0.0%
1990-91	1700	0.3	0.0%
1992	2800	10	22%
1993	2600	50	63%
1994	5800	70	78%
1995	2700	30	78%
1996	0	50	78%
1997-98	0	350	73%
Total	15500	550	

4 Z^0 Pole Detectors

The LEP facility is instrumented with four cylindrical geometry detectors (ALEPH, DELPHI, L3, and OPAL), while the single interaction region of the SLC was instrumented with the upgraded MARK-II detector through 1989, and the SLD detector thereafter. A schematic of the DELPHI detector is shown in Figure 2. The primary components of this detector, fairly typical of the six detectors that have run at the Z^0 , are as follows. Precise charged particle reconstruction is done by a gaseous central tracker, with several precise space points near the IP provided by a silicon μ -strip vertex detector. Calorimetry is mounted inside the magnet coil, outside of which is placed coarse calorimetry and tracking to catch the hadronic tail and identify muons. For the DELPHI and SLD detectors, a Cerenkov ring-imaging detector resides between the tracking and calorimetry to provide dedicated particle identification. Forward instrumentation typically extends the $|\cos\theta|$ coverage to 0.9 or better for tracking and 0.95 to 0.99 for calorimetry. Far-forward position sensitive electromagnetic calorimetry, typically covering the angular region between 20 and 100 mrad, is used to measure the interaction region luminosity via electrons from t-channel Bhabha scattering.

Four advances in instrumentation technique which have been primarily instigated by Z^0 pole physics are discussed in more detail below.

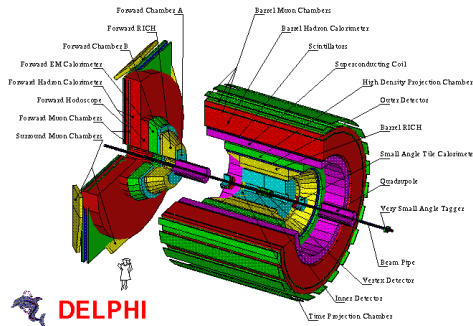


Figure 2. The DELPHI Detector at LEP

4.1 Cylindrical Geometry Silicon Tracking

The first cylindrical geometry silicon μ -strip detector was installed in the MARK-II detector at the SLC in 1989. By 1994 all of the Z^0 pole detectors featured precision silicon tracking, achieving impact parameter resolution at high momentum of better than $20 \mu\text{m}$. The current state-of-the-art silicon tracking device is the SLD pixel CCD detector, shown in two different incarnations in Figure 3. The latest version (VXD3), taking advantage of 8cm silicon wafer technology, comprises three layers between 2.8 and 4.8 cm in r , providing 3 precise 3-d space points out to $|\cos\theta| = 0.85$. The CCD pixel dimension is $22 \times 22 \times 300 \mu\text{m}$, providing a single-hit resolution of approximately $4 \mu\text{m}$. Including the uncertainty in the beam spot location, VXD3 achieves an $r - \phi$ impact parameter resolution of $8 \mu\text{m}$ at high momentum, and $36 \mu\text{m}$ at $p_{\perp} \sqrt{\sin\theta} = 1 \text{ GeV}/c$.

4.2 Cerenkov Ring Imaging Detectors

DELPHI and the SLD contain detectors which detect the photons emitted by charged particles in the well-defined Cerenkov cone as they pass through radiating materials. Photons from a low-threshold, compact liquid radiator are converted in a position-sensitive drift detector filled with a UV-sensitive gas. Photons from a high-threshold gas radiator are imaged back into the drift detector planes by curved mirrors mounted to the outer radius of the Cerenkov detector. The radius of the reconstructed Cerenkov photon ring is a measure of the angle of the Cerenkov cone, and thus the velocity of the radiating particle, which, when combined with momentum measured in the tracking system, provides a measure of the particle's mass. Figure 4

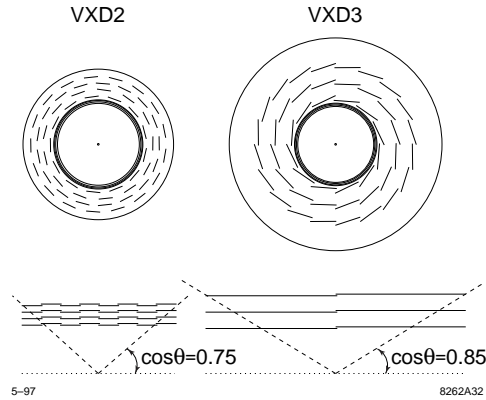


Figure 3. Schematic of the SLD CCD Pixel Tracking Detectors

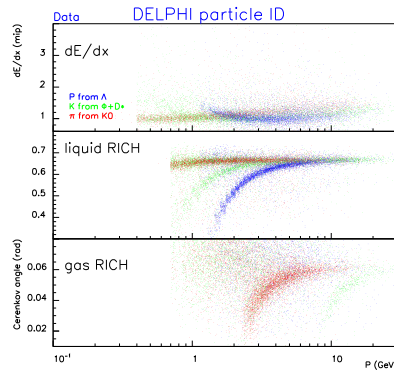


Figure 4. Performance of the DELPHI Particle ID System

shows the performance of the liquid and gas Cerenkov systems, as well as the dE/dX information from the gaseous tracker, for the DELPHI detector. Taken together, these systems provide reliable particle species separation over much of the available kinematic range.

4.3 Electron Beam Polarimetry

The SLD electron beam polarization is analyzed via Compton scattering from a polarized Nd:YAG laser beam. The magnet lattice just downstream of the final focus serves to momentum analyze the scattered electrons, beyond which the scattered electrons are detected in a position-sensitive Cerenkov detector.

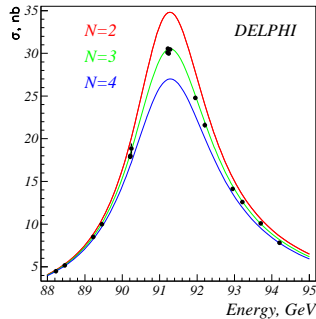


Figure 5. DELPHI Energy Scan Results (N is the number of light ν species assumed).

Table 3. Measured Z^0 Lineshape Parameters

M_Z	$91.1867 \pm 0.0021 \text{ GeV}/c^2$
Γ_Z	$2.4939 \pm 0.0024 \text{ GeV}/c^2$
σ_{had}^0	$41.491 \pm 0.058 \text{ nb}$

The electron beam polarization modulates the observed asymmetry in the Compton cross section between aligned and anti-aligned laser and electron beam polarization, which is measured in the Cerenkov detector as a function of scattered electron energy to a relative precision of $\pm 0.7\%$.

4.4 Precise Luminosity Calibration

The leading-order Bhabha acceptance at small angles is given by

$$\sigma_{e^+e^- \rightarrow e^+e^-} = \frac{1040 \text{ nb} - GeV^2}{s} \left(\frac{1}{\theta_{\min}^2} - \frac{1}{\theta_{\max}^2} \right). \quad (14)$$

Typical acceptance regions of between 20 and 100 mrad lead to cross sections 3-10 times that of the Z^0 peak hadronic cross section. The combination of precise, well-calibrated Si/W calorimeters and higher order calculations of the Bhabha scattering cross-section has led to an overall relative error on the luminosity scale approaching $\pm 0.1\%$.

5 Z^0 Lineshape Measurements

The precise knowledge of the luminosity scale permits a correspondingly precise measurement of the energy dependence of the Z^0 production cross-section, from which accurate values of the lineshape parameters can be extracted. Figure 5 shows the results of such an energy scan, making use of all available off-peak running, from the DELPHI collaboration. Table 3 shows the resulting lineshape parameters, averaged for the four LEP experiments². The relative accuracy on the Z^0 mass (2×10^{-5}) rivals that of the Fermi coupling constant G_F (1×10^{-5}) and thus places a very tight constraint on the value of the weak mixing angle via equation (13).

6 Forward-Backward Asymmetry Measurements

In measuring the forward-backward asymmetries (polarized or unpolarized) there are two basic challenges to be met, both of which are relatively straightforward for final state fermions $f = lepton$. First, the $Z^0 \rightarrow f\bar{f}$ final state of interest must be identified. Secondly, the fermion direction must be determined – usually by finding the thrust axis, and then signing it according to the best estimate of which hemisphere contains the fermion.

Calculating the mass of identified secondary vertices can tag events with heavy final state quarks (b, c) as well as discriminate between the b and c final states themselves. $Z^0 \rightarrow b\bar{b}$ events are tagged in this way with an efficiency as high as 60%, and with a purity as high as 98%. The fermion direction of such ‘inclusively tagged’ events can be determined by the net momentum-weighted hemisphere track charge, the sign of identified kaons from the $b \rightarrow c \rightarrow s$ cascade, or simply the net charge of the tracks forming the vertex. Heavy quark events can be tagged by leptons from semileptonic decay, or by the exclusive reconstruction of a heavy meson state, such as $D^+ \rightarrow K^-\pi^+\pi^+$. For these latter approaches, the charge of the lepton or reconstructed state indicates the charge of the underlying heavy quark.

Figure 6 shows an example of the angular distribution of the estimated b quark direction, in this case for the polarized electron beam at SLAC. Clear forward-backward asymmetries are observed for both left- and right-handed beam, from which the coupling parameter A_b can be measured according to (2) and (10). Table 4 shows the resulting electroweak parameter results from the various forward-backward asymmetry measurements².

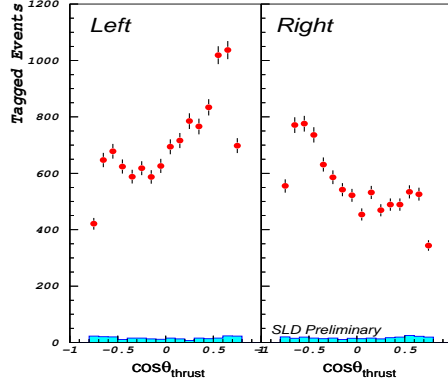


Figure 6. Distribution of the b decay angle in SLD $Z \rightarrow b\bar{b}$ events, separately for left and right handed electron beam.

Table 4. Forward-backward asymmetry measurements and associated extracted electroweak parameters. For the unpolarized asymmetries, the final state coupling parameters A_f are derived under the assumption that $A_e = 0.1489 \pm 0.0017$, which is the LEP/SLC combined value for A_{lepton} .

Observable	Measured Value	Extracted EW Parameter
A_{FB}^l	$.01683 \pm .00096$	$\sin^2 \theta_W = .23117 \pm .00055$
A_{FB}^b	$.0991 \pm .0020$	$\sin^2 \theta_W = .23225 \pm .00037$
A_{FB}^c	$.0713 \pm .0043$	$\sin^2 \theta_W = .2321 \pm .0010$
$A_{FB}^{had} (Q_{FB})$		$\sin^2 \theta_W = .2321 \pm .0010$
\tilde{A}_{FB}^l	$.1456 \pm .0063$	$\sin^2 \theta_W = .2317 \pm .0008$
\tilde{A}_{FB}^b	$.898 \pm .029$	$A_b = .898 \pm .029$
\tilde{A}_{FB}^c	$.634 \pm .027$	$A_c = .634 \pm .027$
A_{FB}^b	See caption	$A_b = .887 \pm .021$
A_{FB}^c	See caption	$A_c = .637 \pm .039$

7 Final State Polarization of τ Leptons

An independent, direct measurement of the parity violation in the Z^0 - τ coupling can be made by measuring the asymmetry in left- and right-polarized τ leptons in $Z^0 \rightarrow \tau\bar{\tau}$ events, which is experimentally accessible via the kinematic distributions of the τ decay products. For example, a diagram of the decay $\tau \rightarrow \nu_\tau \pi(K)$ similar to that of Figure 1 shows that the decay distri-

Table 5. τ Polarization Asymmetry Results

Parameter	Measured Value	Extracted $\sin^2 \theta_W$
A_τ	0.1431 ± 0.0045	0.23202 ± 0.00057
A_e	0.1479 ± 0.0051	0.23141 ± 0.00065

bution in the angle θ^* of the π (K) relative to the τ spin direction in the τ rest frame is proportional to $|\mathbf{d}_{-1/2,1/2}^{1/2}|^2 = \cos^2(\theta^*/2)$. Boosting against the direction of the τ spin (to produce a right-handed τ) results in a distribution

$$\frac{d\Gamma_{RH}^\tau}{dx} \propto x \quad (15)$$

where $x = E_{\pi,K}/E_{beam}$ is the fractional energy of the pseudoscalar decay product. Similarly, for a boost in the direction of the τ spin (to produce a LH τ), the decay angular distribution is proportional to $1 - x$, and so the relative fraction of RH and LH polarized τ 's can be extracted from the x distribution of 1-prong τ decays.

The relation between this τ polarization asymmetry and the electroweak coupling parameters is given by

$$P_\tau(z) = \frac{\sigma_L^\tau(z) - \sigma_R^\tau(z)}{\sigma_L^\tau(z) + \sigma_R^\tau(z)} = \frac{A_\tau(1 + z^2) + 2A_e z}{(1 + z^2) + 2A_\tau A_e z} \quad (16)$$

and so a measurement of $P_\tau(z)$ yields independent values for A_τ and A_e . Table 5 shows the τ polarization results, averaging over all analyzable τ decay modes for the four LEP experiments ².

8 The Left-Right Asymmetry A_{LR}

The left-right asymmetry A_{LR} is measured by simply comparing the number of hadronic Z^0 decays produced with left- and right-handed electron beam:

$$A_{LR} = \frac{1}{|P_e|} \frac{N_{Z^0}^L - N_{Z^0}^R}{N_{Z^0}^L + N_{Z^0}^R}. \quad (17)$$

Corrections due to differences in left- and right-handed beam luminosity, energy, polarization, etc., are small and well understood. With a sample of 550,000 hadronic Z^0 decays produced with $\langle |P_e| \rangle \simeq 72\%$, the SLD experiment finds ²

$$\begin{aligned} A_e = A_{LR} &= 0.1511 \pm 0.0024 \\ \sin^2 \theta_W &= 0.23100 \pm 0.00031. \end{aligned} \quad (18)$$

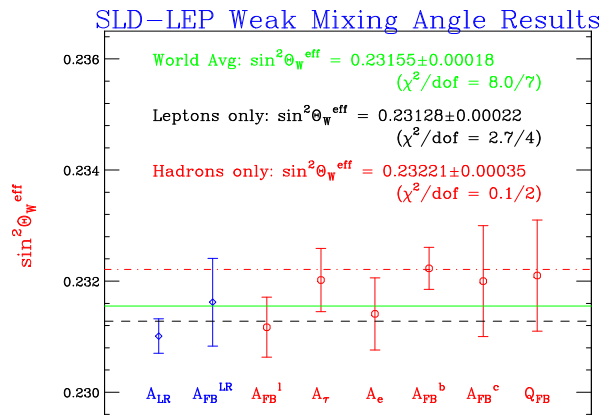


Figure 7. Results for $\sin^2\theta_W$ By Method

Table 6. Partial Width Measurements

Parameter	Measured Value	SM Expectation
R_b	0.2168 ± 0.0007	$0.2155 \pm 0.0003(m_t)$
R_c	0.1694 ± 0.0038	0.1723

In addition to being the single most precise determination of the weak mixing angle, the systematics of this measurement are almost entirely independent of that of other techniques discussed above.

9 Combined Weak Mixing Angle Results and Fits

Figure 7 shows the $\sin^2\theta_W$ results separately for each of the above approaches². While the hypothesis that all of these measurements are consistent with a single mean value is reasonably well supported ($\chi^2 = 8.0$ for 7 d.o.f), there is a mild (2.2σ) discrepancy between the values measured with leptonic final states and those measured with hadronic final states, the latter of which are dominated by the unpolarized A_{FB}^b measurement. Ignoring this issue for the moment, Figure 8 shows a fit for the Higgs Boson mass, assuming the Higgs contributes to radiative loops as prescribed by the Standard Model. At 95% confidence, the Higgs mass is restricted to be below about 270 GeV/ c^2 .

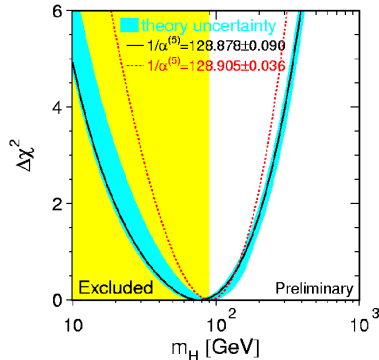


Figure 8. Fit of the SM Higgs Boson mass to electroweak precision data. The solid curve uses as input the value of $\alpha_{\text{em}}(Q^2 = M_Z^2)$ of Ref. [3], while the dashed curve uses that of Ref. [4].

10 Partial Width Measurements

Measurements of Z^0 decay partial widths (12) are particularly sensitive to vertex corrections. Due to the cancelation of both experimental and theoretical uncertainties (luminosity, fiducial volume, effects of gluon radiation, etc.), the partial widths are most cleanly constrained via hadronic branching fractions, e.g. $R_b = \Gamma_{Z^0 \rightarrow b\bar{b}}/\Gamma_{Z^0 \rightarrow \text{had}}$. In addition, with the pure and efficient tags provided by precise silicon tracking, it is possible to constrain the final-state tagging efficiency by comparing the single- *vs.* double-hemisphere tagging rate. The resulting precise constraints on the b and c quark partial widths are shown in Table 6.

11 Fit for $Z^0 - b$ Vertex Parameters

As discussed in Ref. [5], it is interesting to decouple potential anomalous $Z^0 - b$ vertex effects from the vacuum polarization corrections to the weak mixing angle. The explicit $\sin^2 \theta_W$ dependence of the $Z^0 - b$ coupling is removed by writing

$$\begin{aligned}
 \delta s &= [\sin^2 \theta_W]_{\text{meas}} - [\sin^2 \theta_W]_{\text{pred}} \\
 \frac{1}{3} \delta s + \delta g_L^b &= [g_L^b]_{\text{meas}} - [g_L^b]_{\text{pred}} \\
 \frac{1}{3} \delta s + \delta g_R^b &= [g_R^b]_{\text{meas}} - [g_R^b]_{\text{pred}}
 \end{aligned} \tag{19}$$

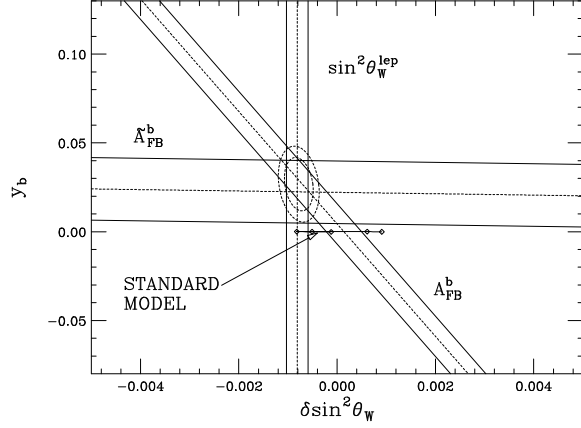


Figure 9. Fit for Z^0-b vertex parameters, projected into the $\delta \sin^2 \theta_W - y_b$ (parity-violation) plane. The Standard Model range includes $169 < m_t < 179 \text{ GeV}/c^2$, and $100 < m_H < 1000 \text{ GeV}/c^2$.

Then, the linear combinations

$$\begin{aligned} x_b &= \cos \phi \delta g_L^b - \sin \phi \delta g_R^b \simeq -\frac{1}{4} \delta R_b \\ y_b &= \sin \phi \delta g_L^b + \cos \phi \delta g_R^b \simeq -\frac{3}{5} \delta A_b, \end{aligned} \quad (20)$$

with $\phi = \tan^{-1} |g_R^b/g_L^b|$, are the deviations from the SM in the Z^0-b vertex partial width (x_b) and parity violation (y_b) strengths. These parameters are constrained by the precision measurements of $\sin^2 \theta_W^{\text{lepton}}$, R_b , R_c , \tilde{A}_{FB}^b , A_{FB}^b , $R_Z = \Gamma_{\text{had}}/\Gamma_{\mu^+\mu^-}$, and σ_{had}^0 . Of particular interest, given the high value of $\sin^2 \theta_W$ from A_{FB}^b , is the projection of this fit into the $(\delta s, y_b)$ plane, shown in Figure 9. It is seen that the high value of $\sin^2 \theta_W$ from A_{FB} (see Table 4 or Figure 7) may possibly be due to an anomalous Z^0-b vertex coupling parameter, a hypothesis which is supported by the direct measurement provided by \tilde{A}_{FB}^b . The overall discrepancy in the strength of Z^0-b coupling parity violation with respect to the SM is just over 2.5σ .

12 Summary and Outlook

With the exception of relatively minor updates to existing results, the picture provided by Z^0 resonance precision measurements is essentially complete. The totality of accumulated data has allowed, with a number of systematically independent approaches, the test of the internal consistency of the Standard

Model to the unprecedented precision of $\delta \sin^2 \theta_W < \pm 0.0002$ – roughly 300 times more accurate than the $\pm \sim 0.06$ available from ν DIS in 1988. While this confirmation of the predictions of the Standard Model is remarkable, there are nonetheless a couple of issues to be noted. A mild discrepancy between the weak mixing angle determined via purely leptonic couplings relative to that made with hadronic couplings could possibly be due to anomalous $Z^0 - b$ vertex effects. This hypothesis is supported, albeit with somewhat inadequate experimental precision, by the SLD direct measurements of the $Z^0 - b$ vertex via the polarized forward-backward asymmetry \tilde{A}_{FB}^b . Secondly, the combination of all electroweak data, assuming only Standard Model contributions to radiative loops, is inconsistent with a heavy Higgs Boson. Should the minimal Standard Model be correct, the Higgs should easily be seen at the LHC, or perhaps earlier in the imminent RUN II of the Fermilab Tevatron.

Acknowledgment

This work was supported in part by the Department of Energy, Grant #DE-FG03-92ER40689.

References

1. A particularly clear presentation of angular momentum and rotation matrix elements is given in Chapter 8 and Appendix H of W. E. Burcham and M. Jobes, *Nuclear and Particle Physics*, Longman Scientific and Technical, 1995.
2. The Z^0 pole electroweak results presented throughout this report have been accumulated in the following two documents, which are products of the LEP Electroweak Working Group (<http://www.cern.ch/LEPEWWG/Welcome.html>): CERN-EP/99-15 and LEPHF 99-01.
3. S. Eidelmann and F. Jegerlehner, *Z. Phys.* **C67**, 585 (1995).
4. M. Davier and A. Höcker, *Phys. Lett.* **B419**, 419 (1998).
5. T. Takeuchi, A. K. Grant, and J. L. Rosner, hep-ph/9409211.